



In vitro single-cell dissection revealing the interior structure of cable bacteria

Zaixing Jiang^{a,b,1}, Shuai Zhang^{a,c,1}, Lasse Hyldgaard Klausen^a, Jie Song^{a,d}, Qiang Li^{a,e}, Zegao Wang^a, Bjørn Torger Stokke^f, Yudong Huang^b, Flemming Besenbacher^a, Lars Peter Nielsen^{g,h}, and Mingdong Dong^{a,2}

^aInterdisciplinary Nanoscience Center, Aarhus University, 8000 Aarhus C, Denmark; ^bDepartment of Polymer Science and Technology, School of Chemistry and Chemical Engineering, Harbin Institute of Technology, 150001 Harbin, People's Republic of China; ^cPhysical Sciences Division, Physical and Computational Sciences Directorate, Pacific Northwest National Laboratory, Richland, WA 99352; ^dInstitute of Nano Biomedicine and Engineering, Shanghai Engineering Research Centre for Intelligent Diagnosis and Treatment Instrument, Department of Instrument Science and Engineering, Shanghai Jiao Tong University, Shanghai 200240, People's Republic of China; ^eSchool of Chemistry and Chemical Engineering, Shandong University, Jinan 250100, People's Republic of China; ^fBiophysics and Medical Technology, Department of Physics, The Norwegian University of Science and Technology (NTNU), NO-7491 Trondheim, Norway; ^gCenter for Electromicrobiology, Aarhus University, DK-8000 Aarhus C, Denmark; and ^hCenter for Geomicrobiology, Section for Microbiology, Department of Bioscience, Aarhus University, DK-8000 Aarhus C, Denmark

Edited by David A. Weitz, Harvard University, Cambridge, MA, and approved July 11, 2018 (received for review May 10, 2018)

Filamentous Desulfobulbaceae bacteria were recently discovered as long-range transporters of electrons from sulfide to oxygen in marine sediments. The long-range electron transfer through these cable bacteria has created considerable interests, but it has also raised many questions, such as what structural basis will be required to enable micrometer-sized cells to build into centimeter-long continuous filaments? Here we dissected cable bacteria cells in vitro by atomic force microscopy and further explored the interior, which is normally hidden behind the outer membrane. Using nanoscale topographical and mechanical maps, different types of bacterial cell-cell junctions and strings along the cable length were identified. More important, these strings were found to be continuous along the bacterial cells passing through the cell-cell junctions. This indicates that the strings serve an important function in maintaining integrity of individual cable bacteria cells as a united filament. Furthermore, ridges in the outer membrane are found to envelop the individual strings at cell-cell junctions, and they are proposed to strengthen the junctions. Finally, we propose a model for the division and growth of the cable bacteria, which illustrate the possible structural requirements for the formation of centimeter-length filaments in the recently discovered cable bacteria.

cable bacteria | atomic force microscopy | dissection | interior structure

Sulfide oxidation is one of the major and most energy-releasing processes in the cascade of aerobic and anaerobic redox processes characterizing the decomposition of organic material in marine sediments (1). Electrons from sulfide to oxygen can be transported through the sediment, and native conductive cable bacteria belonging to the Deltaproteobacteria family Desulfobulbaceae were recently identified as the transporters (2, 3). They form centimeter-long, multicellular filaments, and as living conductors, they inspire the future development of nanobiotechnology and nanobionics (2). The rectangular or rod-shaped cable bacteria are, unlike true filamentous bacteria with unconstricted cell membranes (4), separated by septa. So far, two genera and six species from marine and freshwater habitats have been settled, and giant deep-sea forms and specimens from contaminated aquifers seem to represent additional genera (5–7). The cell size varies considerably between cultures, but the smoothly curved filaments all contain characteristic ridge structures. These ridges are believed to contain strings running longitudinally along the cable bacteria inside a continuous periplasmic space (3). Not much is known about these strings, and a number of intriguing questions about cable bacteria have still not been answered. A key question concerns the structural basis for the microsize bacteria, including how do they divide and how can they form continuous centimeter filament with such surprising stability (3)?

Clinical dissection has been instrumental in providing an understanding of the interior of plants, animals, and humans for thousands of years, and nanodissection is supposed to be a straightforward

approach for exploring the interior of cells and bacteria, which are normally hidden by membranes. Femtosecond laser pulse is an optically based tool to make sub-200-nm-sized cuts, but it is mainly applied in clinical applications and requires precise control of the peak energy of the pulse to avoid collateral damage (8). Focused ion beam is another method applicable for slicing biological cells, and (Cryo)-focused ion beam-based tomography has been developed to reconstruct the 3D structure of single cells (9, 10). However, several steps of focused ion beam are incompatible with the physiological state, and ion damage as well as material redeposited from the beam source might be involved.

Atomic force microscopy (AFM)-based nanodissection is a third option for opening cell membranes. Unlike the optical-based methods, the probe of the AFM is used as a nanoscalpel to perform a purely mechanical dissection/manipulation of biological samples without the risk for side damage or contamination from a beam source (11–13). Furthermore, AFM allows an in situ nanoscale visualization of the dissected structures right after the dissection. After 3 decades of development, AFM has become a widely used tool for characterizing both intra- and extracellular structures with nanoscale resolution in microbiology (14). AFM-based

Significance

Cable bacteria were recently discovered as the facilitators of electron transfer over centimeter distances in marine sediments. In this work, we explore the unique structure of the cable bacteria, using atomic force microscopy-based single-cell in vitro dissection. We identify different types of bacterial cell-cell junctions and continuous dimeric strings hidden under the outer membrane that pass through the cell junctions. The strings seem to serve an important function in maintaining the integrity of individual cable bacteria cells as a united filament. On the basis of our findings, we propose a model for the division and growth of the cable bacteria, which illustrate the possible structural requirements for the formation of centimeter-length filaments in the recently discovered cable bacteria.

Author contributions: Z.J., S.Z., and M.D. designed research; Z.J., S.Z., L.H.K., J.S., Q.L., Z.W., and L.P.N. performed research; Z.J., S.Z., L.H.K., J.S., Q.L., Z.W., and B.T.S. contributed new reagents/analytic tools; Z.J., S.Z., L.H.K., Y.H., F.B., L.P.N., and M.D. analyzed data; and Z.J., S.Z., L.H.K., Y.H., F.B., L.P.N., and M.D. wrote the paper.

The authors declare no conflict of interest.

This article is a PNAS Direct Submission.

Published under the PNAS license.

¹Z.J. and S.Z. contributed equally to this work.

²To whom correspondence should be addressed. Email: dong@inano.au.dk.

This article contains supporting information online at www.pnas.org/lookup/suppl/doi:10.1073/pnas.1807562115/-DCSupplemental.

Published online August 6, 2018.

nanodissection has furthermore been applied to investigate the structure of cell-membrane proteins (15–17), chromosomes (18, 19), and viruses (20, 21). AFM is also a promising technique for recognizing the functional structures inside bacterial cells (22, 23) and the self-assembly of submembrane layers (24, 25), which are normally hidden by the cell envelope. AFM can also be used as an advanced multiparametric visualization technique, in which topographic variations are correlated to a corresponding mechanical response of the microorganism (26, 27). Using a functionalized tip, the multiparametric AFM can probe binding mechanisms of bacterial biofilms (28, 29) and localizes the active receptor/vulnerable positions on cells (30) and bacteria (31).

Here, three kinds of junctions among individual cable bacteria cells were identified based on various AFM topographies. We in vitro dissected the cable bacteria cells individually via AFM-based nanodissection. We further applied AFM-based dynamic nanomechanical mapping (27, 31, 32) to explore the interior of cable bacteria in situ, which is inaccessible to most quantitative nanovisualization techniques. Strings underneath the outer membrane (OM), along the long axis of bacterial cells, were identified and found to be continuous throughout the cable bacteria cells. An architecture consisting of OM ridges enclosing single strings at the cell–cell junctions was found. These architectures, attached on the inside surface of OM, are rare in other kinds of filamentous bacterial species. They are proposed to strengthen the cell–cell junctions and increase their robustness. Based on AFM data and supplementary data, we propose a model to describe the possible division and growth cycle of cable bacteria. It also illustrates the structure of the strings and OM and expounds their corresponding functions in filamentous maintenance, division, and elongation. This is an important step in understanding the interior structural requirement to form bacterial cables, and it also provides an exciting opportunity for describing the growth and division of a recently discovered type of bacteria.

Results

Three Distinct Kinds of Cell–Cell Junctions Were Identified by AFM Topography. Marine sediment from the top 20-mm layer was gently washed, whereby filamentous bacteria were separated out and became apparent under the optical microscope. They were further characterized by FISH with a specific 16S rRNA-targeting probe and DAPI probe (Fig. 1*A*). The individual bacterial cells can be identified, and the junction between each cell is apparent (the dashed square in Fig. 1*A*). However, because of the resolution limitations of light microscopy, it is challenging to obtain more structural details of the filamentous bacteria. AFM was then used to investigate the finer structure of the bacterial junctions, and excitingly, it was able to identify three distinctive groups of cell–cell junctions based on the ratio (r) between the bacterial cell body diameter and the junction diameter. Representative AFM topography images are presented in Fig. 1*B–D*. It is obvious that r of *J1* is much bigger than 1, whereas that of *J2* is much smaller than 1, and that of *J3* is roughly equal to 1. Comparison of line profiles clearly shows the difference in topographies (Fig. 1*E–G*), which could also be observed by scanning electron microscopy (SEM; *SI Appendix, Fig. S1*). AFM and SEM both show the existence of continuous ripples in the membrane; investigating these further requires looking into the interior of the cells.

The Cell Junctions and Bodies Are Proposed to Have Different Robustness. One *J1* junction between two nearby bacterial cells was deformed by the probe along the direction indicated by the white arrow (Fig. 2*A* and *B*). It is obvious that the junction was compressed along the pushing direction, but survived without obvious wounds or break across the junction. This indicates that the junction is capable of surviving under certain cross-section-applied forces. It ensures that the bacterial filament is able to elongate along the length over hundreds/thousands of cells.

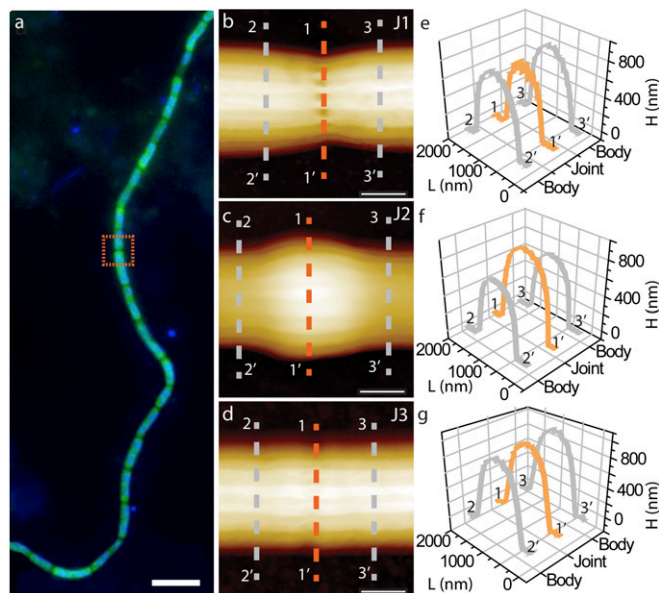


Fig. 1. The overview of bacterial cable and different junctions between two bacteria cells. (*A*) Micrograph showing filamentous *Desulfobulbaceae* extracted from a glass bead section and hybridized with a specific ELF654 FISH and DAPI probe. The dashed square indicates the junctions. (Scale bars, 5 μm .) (*B–D*) AFM topography images of different kinds of junctions, depending on the ratio between the diameters of bacteria cell and junctions. (Scale bars, 300 nm.) (*E–G*) The corresponding line profiles marked on *B–D* to show the different diameters of the junctions compared with those of bacteria cells, respectively.

Then, the AFM probe was used to scratch holes in the bacteria by applying different forces to OM (Fig. 2*C* and *D*). The applied forces were increased gradually from the top of Fig. 2*D* to the bottom on the arrows' positions. The comparison of the images before and after manipulation (Fig. 2*C* and *D*), as well as line profiles (Fig. 2*G*, *H*, and *J*), proves that there is a certain applied force threshold of OM; unless the applied force is strong enough (similar to the black arrows in Fig. 2*D* and *J*), OM is able to resist the mechanical scratch. It indicates the cable bacteria cells might have strong skeleton structures underneath OM.

The Cell–Cell Junctions Mechanically Isolate Neighboring Bacterial Cells. In Fig. 2*C* and *D*, when the cell on one side of junction *B* (*J1*) was broken, the cell on the other side still retained its structure. A comparison of the line profiles shows that the height and diameter of the bacterial cell is unchanged by the dissection (Fig. 2*G*). This means that the cell contents on the two sides of a junction are well separated. This matches sectional TEM data (the white arrows in *SI Appendix, Fig. S2*), in which both an inner membrane between cells and a continuous outer membrane at a junction between two cells is visible. More important, we found the junction has much higher applied force threshold compared with the cell body, seeing as how the junction survived even under the highest applied force (orange arrow on the γ - γ' line in Fig. 2*D*), without change in height and diameter (Fig. 2*J*). When the applied force was further increased a whole bacterial filament could be nearly completely dissected along the length (Fig. 2*E*, *F*, and *K–M*), but the junctions still kept their shape (Fig. 2*L*). These findings all seem to confirm that the cable bacteria cells are well delineated and yet tightly connected in a continuous filament structure, and the filament can resist considerable negative mechanical distortions from the surroundings.

Nano-Dissection and Quantitative Nanomechanical Mapping Confirm the Existence of Strings Under OM. The inner side of a piece of bacterial OM, isolated by AFM-based nanodissection, was characterized by

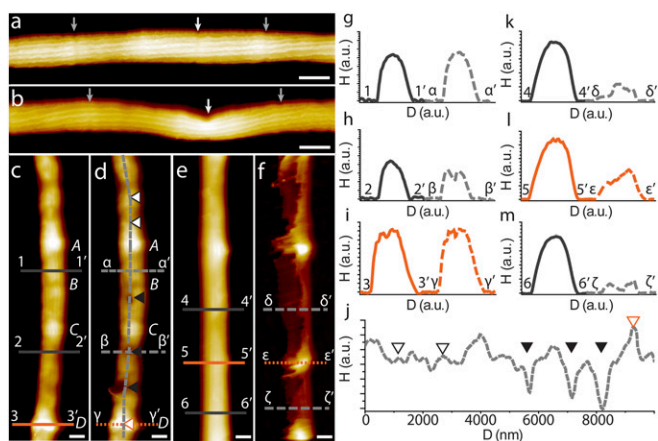


Fig. 2. Nanodissection to cable bacteria. (A and B) AFM topography images recorded before and after pushing the junction by AFM-tips along the substrate. The white arrows indicate the manipulated junctions, and the light gray ones show the references between the two images. (C and D) AFM topography images recorded before and after dissecting holes with different applied force perpendicular to the substrate. The arrows indicate the dissection positions, and A–D indicate four cell–cell junctions. (E and F) AFM topography images recorded before and after dissecting another segment of cable bacteria along the long axis of the filament. (G–M) the corresponding line profiles marked on C–F to show the results of nanodissection, which indicates the various strength on cells and junctions. (N) The dark gray dashed line along the filamentous bacteria in D and arrows correspond to the ones in the image. (Scale bars, 500 nm.)

dynamic nanomechanical mapping. The topography and corresponding Young's modulus map are shown in Fig. 3A. From the line profile along the dashed line $\alpha\alpha'$ (Fig. 3A and B), specific structures underneath the OM are apparent (highlighted by the

arrows in Fig. 3A and column 2 on Fig. 3B). The structures are named as strings and have a thickness of ~ 20 –40 nm. From the topographical point of view, the strings are higher than the OM and the glass slide (indicated by column 3 and column 1, respectively). The accuracy of the modulus values can be only considered under certain assumptions. The Sneddon model is applied to calculate the modulus (27), and in addition, the calculated modulus is slightly overestimated because of the substrate effect. However, the relative stiffness difference can be easily identified in Fig. 3C. From the elastic modulus point of view, the strings are softer. A histogram of the Young's modulus distribution on the selected area in Fig. 3A presents the population of strings much clearer as softer than the OM and glass slide (Fig. 3C). This kind of subcellular architecture is found to be normal in the cable bacteria (SI Appendix, Fig. S3).

The Strings Display a Twisted Dimeric Structure. String S1 and S2 are examples of the dimeric structure of the strings seen at higher magnification (Fig. 3D). Compared with S2, the left end of S1 looks to have been distorted by the probe, and the two substrings are separated from each other. Furthermore, the two substrings may twist around each other, but without specific period, as pointed out by the dashed arrows in Fig. 3D. Structural variations are able to tune the readout of Young's modulus of the same material (33), and it is possible that the twisting parts and untwisting parts have different modulus. The color contrast of Fig. 3D proves this proposal, and by fitting the height and modulus distributions of Fig. 3D, the twisting phenomenon becomes much more straightforward (Fig. 3E and F). The twisted parts are higher, but softer, than the untwisted parts of the strings. SI Appendix, Fig. S3 shows sets of topography and corresponding Young's modulus maps of strings from different bacteria. The images show that S1 and S2 are not rare examples, and that the strings generally have a helical dimer structure. TEM tomography data furthermore supports the nanodissection

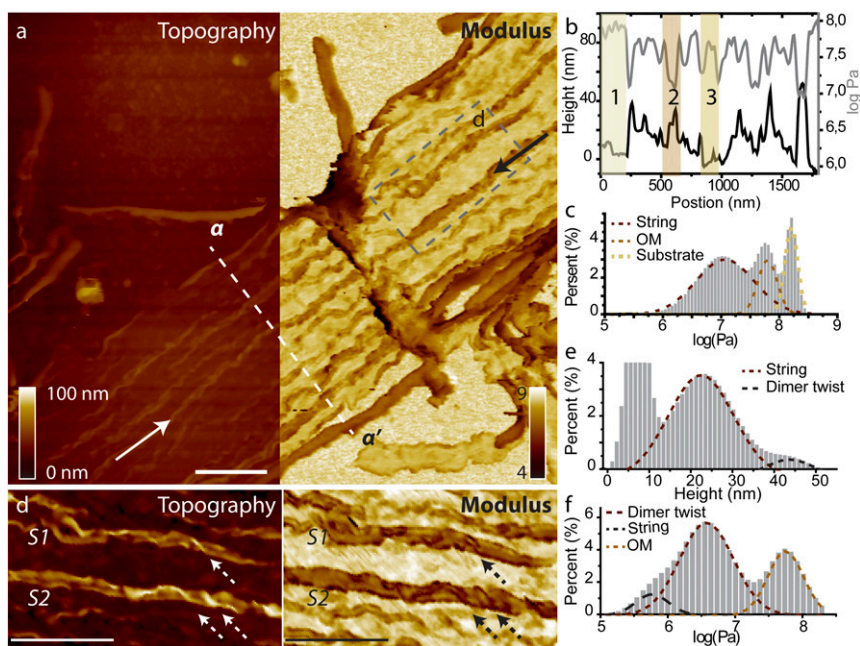


Fig. 3. Correlated topography and Young's modulus maps of the interior bacterial OM by dynamic quantitative nanomechanical mapping, after in situ nanodissection. (A) AFM topography (Right) and Young's modulus (Left) map of inside of OM after nanodissection. The two arrows indicate one of the strings, which are hidden underneath the OM in the normal state. (B) The two line profiles along $\alpha\alpha'$ in A extracted from topography (black) and Young's modulus (gray) maps, respectively. (C) Distribution of elasticity in the selected areas on the Young's modulus map of A showing the different elasticities between OM and strings. (D) Topography map and corresponding Young's modulus map zoomed-in from the gray dashed square in A. They indicate two types of possible strings after nanodissection, with the arrows highlighting the possible twisting events along the strings. (E) Height distribution of the topography map in D indicating the existence of twisted dimers along strings. (F) Distribution of the Young's modulus map in D indicating the existence of twisted dimers along strings. (The scale bars in A and D indicate 500 nm length.)

data (*SI Appendix, Fig. S2* and *Movie S1*), as at a certain section slice, the twisted outline of the string can be identified. The OM has furthermore been proposed to shape into the ridges between strings, creating a durable structure (3).

The Strings Are the Key Structure to Connect the Individual Bacterial Cells Along the Continuous Filament. Two pieces of completely opened OM by nanodissection were captured by dynamic nanomechanical mapping (Fig. 4*A* and *SI Appendix, Fig. S4*). The inner membrane and the encapsulated cytoplasm were gone. Interestingly, not all the junctions have been opened. On the basis of the diameters of the unopened junctions and the outlines of the envelope linking to them, we observe that junctions of the J1 kind (highlighted by dashed arrows in Fig. 4*A*) keep the shape, but J2 junctions are opened (highlighted by solid white arrows in Fig. 4*A*). However, because of the surface characterization technique nature of AFM, standard topography does not have strong specificity, and it is difficult to show the interior structural information of the unopened J1 ones. Hence, the deformation data obtained by dynamic nanomechanical mapping were extracted to help understand the detailed structure of junctions. Fig. 4*B* shows a higher-resolution deformation map zoomed from Fig. 4*A* and represents the deformation of the various species produced by the same applied force, and it is obvious that different species show specified contrasts and that the gradient order of them is not the same as that in the topography image. Two typical junctions in Fig. 4*B* were further magnified to investigate the details of this. Fig. 4*C* shows a junction considered to be J2 because it has been opened completely after the nanodissection. After drawing the height contour lines on it, the detailed structures in such a junction are clarified. It is straightforward to see that the strings (the dashed arrows in Fig. 4*C*) pass through the junction continuously from one bacterial cell to the other one. Returning to Figs. 3*A* and 4*A*, it is obvious that the continuous strings connect several bacterial cells. This supports the proposal that the strings can be a centimeter long, capable of linking the individual cable bacteria cells along the filament.

The Strings at Cell–Cell Junction. Fig. 4*C* also shows particle-like features at the inner-side of cell–cell junction that are arranged in a necklace structure at J2, where the particle-like features and strings sit next to each other at the junction. The corresponding deformation map of Fig. 4*C* (Fig. 4*D*) also presents the continuous strings passing through the junction. The contrast and quantitative deformation distributions of Fig. 4*D* clearly show strings and particle-like features apart from the bacterial OM. This means that the ordered particle-like features and continuous strings have different mechanical properties from the OM. More important, according to the corresponding deformation map of J1 (Fig. 4*F*), particle-like features embedded in the aggregation can still be distinguished (the gray arrows in Fig. 4*F*). Overlaying the deformation contour lines of Fig. 4*F* on top of Fig. 4*E* validates that the continuous strings pass through the junction and through the particles. This means that even though the overall topography of J1 and J2 is different, they still share the same inner structure. And comparing the deformation distributions deduced from J1 and J2, respectively (Fig. 4*G* and *H*), the same kind of structures can be found with similar deformation under the same range of applied force.

Discussion

By integrating the AFM data of the dissected bacteria and the TEM 3D tomography of cable bacteria filament along the length axis (*Movie S1*), we propose a model to represent the interior structure of cable bacteria (Fig. 5*A*). The different types of junctions (J1, J2, and J3) also may refer to various stages of bacterial cell division. Previous studies have shown that the cable bacteria growth is too rapid to be apical, evidencing an exponential growth with continuous division of all cells within the filament (34). This makes the cable bacteria growth process additionally noteworthy, as the strings must be continuously elongated within the bacterial cable. Accumulation of FtsZ was furthermore observed at cell–cell junctions (*SI Appendix, Fig. S5*), which might indicate that an FtsZ ring is formed similar to nonfilamentous bacterial division. String-like structures of FtsZ

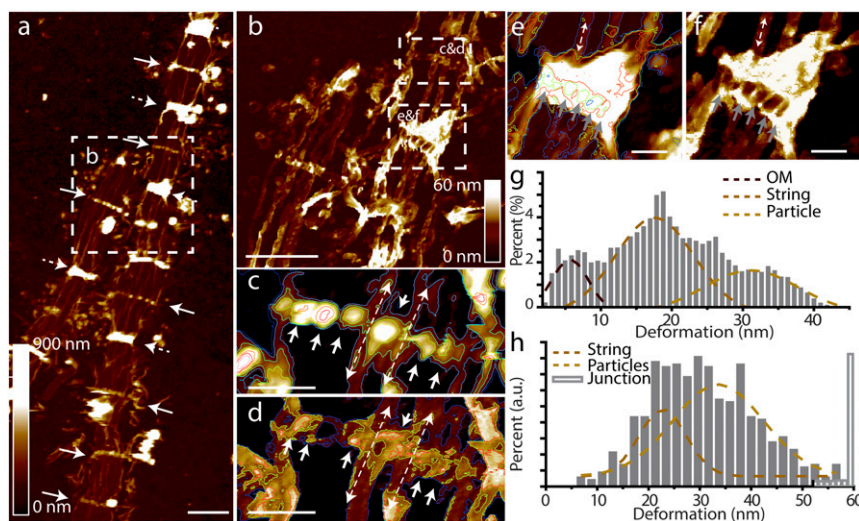


Fig. 4. The details about the different junctions revealed by dynamic quantitative nanomechanical mapping after nanodissection. (A) AFM topography maps of two pieces of inner side OM, isolated by nanodissection. The solid and dashed arrows indicate two kinds of junctions, respectively. (B) Deformation map of the inner side OM, zoomed-in from A. (C and D) High-resolution topography and corresponding deformation maps of J2 junctions with contour lines, zoomed from B. The long dashed arrows indicate the string passing through junction to connect two nearby bacterial cells along the length. The solid arrows highlight the particle-like features aligned at the junction, perpendicular to the length of filamentous bacteria. (E and F) High-resolution topography map of J1 junction with deformation contour lines, and the corresponding deformation map, zoomed from B. The topography map was overlapped with the contour line of the corresponding deformation map. The dashed arrow indicates the continuous string through the junction, and the gray arrows highlight the particle-like features. Color scale for topography and deformation match that of A and B, respectively. (G and H) Deformation distributions of D and F, respectively. (Scale bars in A and B, 2 μm length; C–F, 500 nm length.)

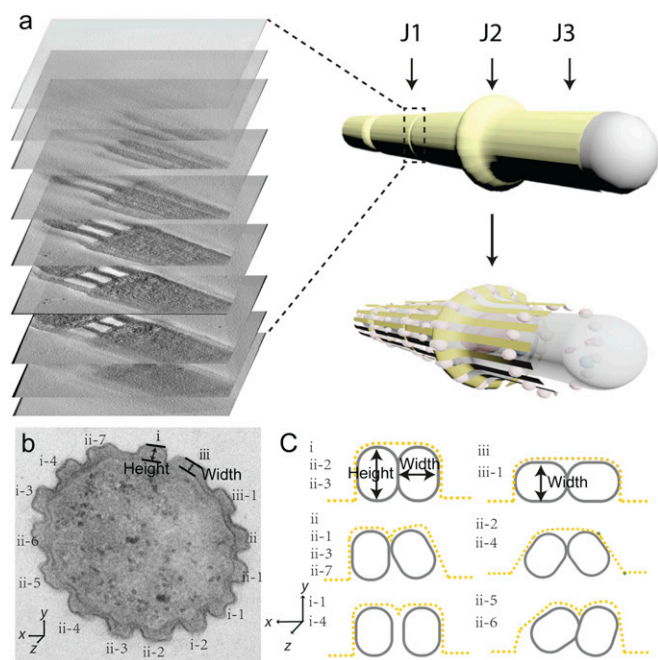


Fig. 5. Proposed model of cable bacteria interior structure. (A, Left) Z-stack of representative TEM images of cable bacteria filament, extracted from the TEM 3D tomography. (Right) Model of the exterior of the filament and the bacterial components after peeling off the OM. (B) Cross-section TEM image of bacteria; the various cross-sections of OM ridges have been classified into different possible patterns. (C) Proposed general string twisting patterns corresponding to the dimer string: Pattern i: two substrings in parallel arrangement. Pattern ii: two substrings in a certain angle arrangement. Pattern iii: two substrings in vertical arrangement.

have been observed with filamentous growth of *Escherichia coli* (35), but the fluorescent images show that the cable bacteria strings are unlikely to contain FtsZ protein. On the basis of our results, we speculate how the three types of junction fit into the cell division process: first, as the cell division starts, chromosomes are replicated and division proteins produced. This will lead to an increase of cellular volume. Hence, the middle of the dividing bacterial cell may start to swell, whereas a new junction is formed. We propose J2 as junctions undergoing this step where replication is beginning. With the division, two new bacterial cells will form. The filament elongates again and J2 shrinks back to J1, which becomes the mature junction. According to this model, J3 is a transitional type of junction, in which a septum is forming between the two cells. Both Fig. 4A and SI Appendix, Fig. S4 show J1 and J2 appearing in an alternating manner; this matches an exponential growth with uniform division of all cells according to the proposed division model. In some cases, the appearance of J2 was not frequent; this might be associated with differing reproductive capacities of cable bacteria, depending on the environment of the filament.

The nanodissection data (Fig. 2) provide evidence that the mature cell–cell junctions (J1) are sealed, and cable bacteria cells, contrary to other multicellular filamentous bacteria, do not form a joint outer sheath. The oblique section TEM images of the cell–cell junction indicate that the OM shrinks at the normal cell–cell junction (3); hence, very sharp gullies form between each two OM ridges facing inward toward the filament. The strings are located in the ridges, and they are guided through the cell–cell junction by the ridge structure. These speculations also explain the occurrence of particle-like features at the junction in Fig. 4. Once the outer membrane was dissected, the AFM probe was used to scan the inside surface of the OM in Fig. 4. The

geometry of the gully should be furthermore deformed by the AFM probe, differentiating it from a piece of the OM.

It is well known that the bacterial cell membrane, or cell wall, is responsible for determining the shape of the cell by overcoming the difference in osmolality on the two sides. The architectures on the cell envelope have been studied by AFM on selected bacterial species (22, 23, 36–38). In the case of cable bacteria, strings that attach on the inside of OM ridges seem to have a key role in structuring the bacterium. They orient along the long axis of the bacterial cell, contrary to normal structures orienting along the short axis (37), and they are able to continue over many cells. Using AFM dissection, we find that the strings have a diameter of 10–30 nm, and that they possess a twisted structure (SI Appendix, Fig. S3). The size of the strings is similar to microtubules, which are known to exist in both mammalian cells and some bacteria, where they maintain the structural identity of the cell (39). Our mechanical tests (Fig. 2) show that strings can strengthen the OM and junctions of cable bacteria; the strings thus serve a similar function to microtubules. The twisted dimer structure of the strings is important in improving the robustness of cable bacteria. It is well known that amyloid peptides quite often self-assemble into twisted amyloid fibrils that contain different numbers of subfibrils (40). Amyloid fibrils generally display outstanding mechanical properties, and the twisted structure might be a part of this (41). Hence, we speculate that the twisted-dimer strings are an essential tool for cable bacteria to resist stresses from the surroundings and maintain a centimeter length. However, unlike amyloid fibrils, the twisted dimer structures of the strings are not periodic. This explains the finding that the cross-sections of the OM ridges show irregular shapes in TEM images, as the shape of the cross-section depends on its position along the nonperiodic twisted dimer structure. (Fig. 5B and C) Although the chemical nature of the strings has not been identified, this work provides an important insight into the functionalities of the strings to elongate along cable bacteria filament, linking individual cells together (Fig. 4E and F) and strengthening the cell–cell junctions. The dimer architecture of the strings bonded to the OM may be important for the strength and robustness of the cable, and could hint toward an evolutionary origin.

In summary, the interior structure of the recently discovered cable bacteria has been surveyed in vitro on single-cell level. Three kinds of cell–cell junctions and strings underneath the OM have been identified and understood via AFM-based nanodissection. These identified bacterial architectures, strings, are supposed to be the structural base for the growth of cable bacteria filaments over centimeter distances. Furthermore, a possible division cycle of cable bacteria has been proposed. Both of these findings are important for furthering our understanding of this identified bacterial species and for culturing and mimicking cable bacteria as bio-conductors in nanobiotechnology.

Methods

Bacterial Culture. The bacteria were obtained from sulfidic sediment sampled in Aarhus Bay, Denmark. The sediment was sieved, transferred to glass core liners, and incubated for 3–4 wk in aquaria with circulating air saturated sea water, as described previously (42). The bacterial filaments were further picked, cut, and immobilized on Polysine glass slides (Menzel-Gläser) in filtered seawater. The whole process follows the protocol in ref. 3.

FISH Identification. Nucleic acids were extracted from sediment and glass microspheres, and from single filaments collected by micromanipulation. RNA was reverse-transcribed, and 16S rRNA cDNA fragments were PCR-amplified, cloned, and sequenced. Oligonucleotide probes for FISH were designed specifically for the retrieved sequences and used for microscopic identification and quantification of the filamentous *Desulfobulbaceae* by FISH in fixed sediment samples. The whole process follows the protocol in ref. 3.

AFM-Based Nano-Dissection. The glass slides with immobilized cable bacteria were loaded on a Dimension FastScan AFM (Bruker), and the dissection was controlled by NanoMan software (Bruker) with FastScan B probe ($k \sim 1.8$ N/m; Bruker). During nanodissection of a bacterial filament, AFM was operated in contact mode. The applied force by the probes was controlled by different z-piezo move distances. In general, an applied z-piezo movement (z_m) of 400 nm was able to break OM of bacterial filamentous. The applied lateral force should be much larger than several hundreds of nano-Newton, even in micro-Newton range (43). All of the experiments were performed in nuclease-free water (Ambion)

Quantitative Nanomechanical Mapping. The dissected cable bacteria on the glass slide were characterized with Dimension FastScan (Bruker) in PeakForce QNM mode. FastScan-C probe was used, and each probe was calibrated according to the released notes from Bruker. Young's modulus was fitted using the Sneddon model. The experiment was performed in nuclease-free water. All images were further processed and analyzed by SPIP and topoStich (Image Metrology ApS).

SEM. Subsamples retrieved from the glass bead layer in cores from glass bed incubations were carefully deposited onto carbon tape. Samples were then rinsed in milli-Q water and air-dried. SEM images were obtained on a NanoSEM (FEI, Nova 600 NanoSEM) operated in low-vacuum (60 Pa) and low-voltage (3 kV) mode to apply the charge contrast imaging data.

TEM. Single filaments were micromanipulated from sediment samples and transferred to centrifuge tubes. The bacterial suspension was then centrifuged at $22 \times g$ for 30 s. The pellet was then covered with a small droplet of 10% gelatin, gently mixed, and hereafter fixed in 2% glutaraldehyde. After this step, the samples were embedded in resin. Ultrathin sections were cut

on an Ultramicrotome Leica Ultracut UCT (Leica Mikrosysteme GmbH), using a 45-g diamond knife (Diatome). Samples with thickness of 200 nm were placed on a 200 mesh nickel grid and covered with carbon. Grids were then loaded into a commercial transmission electron microscope (FEI Titan Krios), which was operated at 300 kV. The specimen was tilted in $\sim 2^\circ$ increments over a total angular range of $\pm 60^\circ$ along the x and y axis, respectively. All the images were kept by using automated data acquisition software. 3D reconstructions from the above tilt series were performed with the weighted back-projection method, and further analysis of tomograms was performed using IMOD software (44).

ACKNOWLEDGMENTS. This research was supported by grants from the Danish National Research Foundation, Aarhus Universitets Forskningsfond (AUFF NOVA-project), Villum Foundation, Lundbeck Foundation, and EU H2020 RISE 2016 (MNR45Cell 734174 project). Z.J. acknowledges National Program for Support of Top-notch Young Professionals, China Aerospace Science and Technology Corporation-Harbin Institute of Technology Joint Center for Technology Innovation Fund (HIT15-1A01), and Harbin city science and technology projects (2013DB4BP031 and RC2014QN017035). S.Z. acknowledges the support from the Materials Synthesis and Simulation Across Scales Initiative through the Laboratory Directed Research and Development program at Pacific Northwest National Laboratory. Pacific Northwest National Laboratory is a multiprogram national laboratory operated for Department of Energy by Battelle under Contract DE-AC05-76RL01830. J.S. acknowledges financial support from National Science Foundation of China (21605102) and Thousand Youth Talents Plan. B.T.S. acknowledges support from Norges Teknisk-Naturvitenskapelige Universitet institutional support. L.H.K. acknowledges support from the Carlsberg Foundation Internationalization fellowships (CF16-0757). L.P.N. acknowledges grants from The Danish Council for Independent Research/Technology and Production.

- Jørgensen BB (2000) Bacteria and marine biogeochemistry. *Marine Geochemistry*, eds Schulz HD, Zabel M (Springer, Berlin), pp 173–207.
- Nielsen LP, et al. (2017) Bacterial conductive fibres. European Patent (EPO) 2647727:B1. (November 1, 2017).
- Pfeffer C, et al. (2012) Filamentous bacteria transport electrons over centimetre distances. *Nature* 491:218–221.
- Willey JM, Sherwood LM, Woolverton CJ (2010) *Prescott's Microbiology* (McGraw-Hill Education, Columbus, OH).
- Trojan D, et al. (2016) A taxonomic framework for cable bacteria and proposal of the candidate genera Electrothrix and Electroneuma. *Syst Appl Microbiol* 39:297–306.
- Kato S, Yamagishi A (2016) A novel large filamentous deltaproteobacterium on hydrothermally inactive sulfide chimneys of the Southern Mariana Trough. *Deep Sea Res Part I Oceanogr Res Pap* 110:99–105.
- Müller H, et al. (2016) Long-distance electron transfer by cable bacteria in aquifer sediments. *ISME J* 10:2010–2019.
- König K, Riemann I, Fritzsche W (2001) Nanodissection of human chromosomes with near-infrared femtosecond laser pulses. *Opt Lett* 26:819–821.
- Heymann JAW, et al. (2009) 3D imaging of mammalian cells with ion-abrasion scanning electron microscopy. *J Struct Biol* 166:1–7.
- Rigort A, et al. (2012) Focused ion beam micromachining of eukaryotic cells for cryo-electron tomography. *Proc Natl Acad Sci USA* 109:4449–4454.
- Müller DJ, Dufrène YF (2008) Atomic force microscopy as a multifunctional molecular toolbox in nanobiotechnology. *Nat Nanotechnol* 3:261–269.
- Obataya I, Nakamura C, Han S, Nakamura N, Miyake J (2005) Nanoscale operation of a living cell using an atomic force microscope with a nanoneedle. *Nano Lett* 5:27–30.
- Scheuring S (2006) AFM studies of the supramolecular assembly of bacterial photosynthetic core-complexes. *Curr Opin Chem Biol* 10:387–393.
- Xiao J, Dufrène YF (2016) Optical and force nanoscopy in microbiology. *Nat Microbiol* 1:16186.
- Müller DJ, Schoenberger CA, Büldt G, Engel A (1996) Immuno-atomic force microscopy of purple membrane. *Biophys J* 70:1796–1802.
- Scheuring S, Rigaud JL, Sturgis JN (2004) Variable LH2 stoichiometry and core clustering in native membranes of *Rhodospirillum rubrum*. *EMBO J* 23:4127–4133.
- Scheuring S, et al. (2004) Watching the photosynthetic apparatus in native membranes. *Proc Natl Acad Sci USA* 101:11293–11297.
- Thalhammer S, Stark RW, Müller S, Wienberg J, Heckl WM (1997) The atomic force microscope as a new microdissecting tool for the generation of genetic probes. *J Struct Biol* 119:232–237.
- Fotiadis D, Scheuring S, Müller SA, Engel A, Müller DJ (2002) Imaging and manipulation of biological structures with the AFM. *Micron* 33:385–397.
- Ivanovska IL, et al. (2004) Bacteriophage capsids: Tough nanoshells with complex elastic properties. *Proc Natl Acad Sci USA* 101:7600–7605.
- Roos WH, Wuite GJL (2009) Nanoindentation studies reveal material properties of viruses. *Adv Mater* 21:1187–1192.
- Plomp M, Leighton TJ, Wheeler KE, Hill HD, Malkin AJ (2007) In vitro high-resolution structural dynamics of single germinating bacterial spores. *Proc Natl Acad Sci USA* 104:9644–9649.
- Turner RD, Hurd AF, Cadby A, Hobbs JK, Foster SJ (2013) Cell wall elongation mode in Gram-negative bacteria is determined by peptidoglycan architecture. *Nat Commun* 4:1496.
- Chung S, Shin S-H, Bertozzi CR, De Yoreo JJ (2010) Self-catalyzed growth of 5 layers via an amorphous-to-crystalline transition limited by folding kinetics. *Proc Natl Acad Sci USA* 107:16536–16541.
- Shin S-H, et al. (2012) Direct observation of kinetic traps associated with structural transformations leading to multiple pathways of 5-layer assembly. *Proc Natl Acad Sci USA* 109:12968–12973.
- Dufrène YF, Martínez-Martin D, Medalsy I, Alsteens D, Müller DJ (2013) Multiparametric imaging of biological systems by force-distance curve-based AFM. *Nat Methods* 10:847–854.
- Zhang S, Aslan H, Besenbacher F, Dong M (2014) Quantitative biomolecular imaging by dynamic nanomechanical mapping. *Chem Soc Rev* 43:7412–7429.
- Formosa-Dague C, Speziale P, Foster TJ, Geoghegan JA, Dufrène YF (2016) Zinc-dependent mechanical properties of *Staphylococcus aureus* biofilm-forming surface protein SasG. *Proc Natl Acad Sci USA* 113:410–415.
- Formosa-Dague C, et al. (2016) Sticky matrix: Adhesion mechanism of the Staphylococcal polysaccharide intercellular adhesin. *ACS Nano* 10:3443–3452.
- Alsteens D, et al. (2017) Nanomechanical mapping of first binding steps of a virus to animal cells. *Nat Nanotechnol* 12:177–183.
- Alsteens D, Trabelsi H, Soumillion P, Dufrène YF (2013) Multiparametric atomic force microscopy imaging of single bacteriophages extruding from living bacteria. *Nat Commun* 4:2926.
- Xia D, et al. (2014) Hydrated human corneal stroma revealed by quantitative dynamic atomic force microscopy at nanoscale. *ACS Nano* 8:6873–6882.
- Zhang S, et al. (2013) Coexistence of ribbon and helical fibrils originating from hI-APP20–29 revealed by quantitative nanomechanical atomic force microscopy. *Proc Natl Acad Sci USA* 110:2798–2803.
- Schauer R, et al. (2014) Succession of cable bacteria and electric currents in marine sediment. *ISME J* 8:1314–1322.
- Mileykovskaya E, Sun Q, Margolin W, Dowhan W (1998) Localization and function of early cell division proteins in filamentous *Escherichia coli* cells lacking phosphatidylethanolamine. *J Bacteriol* 180:4252–4257.
- Turner RD, et al. (2010) Peptidoglycan architecture can specify division planes in *Staphylococcus aureus*. *Nat Commun* 1:26.
- Hayhurst EJ, Kailas L, Hobbs JK, Foster SJ (2008) Cell wall peptidoglycan architecture in *Bacillus subtilis*. *Proc Natl Acad Sci USA* 105:14603–14608.
- Andre G, et al. (2010) Imaging the nanoscale organization of peptidoglycan in living *Lactococcus lactis* cells. *Nat Commun* 1:27.
- Lodish H, et al. (2000) Cell motility and shape II: Microtubules and intermediate filaments. *Molecular Cell Biology*, eds Lodish H, Berk A (W. H. Freeman, New York), pp 793–847.
- Adamcik J, et al. (2010) Understanding amyloid aggregation by statistical analysis of atomic force microscopy images. *Nat Nanotechnol* 5:423–428.
- Knowles TPJ, Buehler MJ (2011) Nanomechanics of functional and pathological amyloid materials. *Nat Nanotechnol* 6:469–479.
- Nielsen LP, Risgaard-Petersen N, Fossing H, Christensen PB, Sayama M (2010) Electric currents couple spatially separated biogeochemical processes in marine sediment. *Nature* 463:1071–1074.
- Green CP, et al. (2004) Normal and torsional spring constants of atomic force microscope cantilevers. *Rev Sci Instrum* 75:1988–1996.
- Kremer JR, Mastrorade DN, McIntosh JR (1996) Computer visualization of three-dimensional image data using IMOD. *J Struct Biol* 116:71–76.